RESEARCH ARTICLE | MARCH 19 2025

Optimal generation of mesoscopic twin-beam states by means of a natively femtosecond laser system

A. Pozzoli ; M. Lamperti ; M. Clerici ; M. Bondani ; A. Allevi

APL Photonics 10, 036116 (2025)
https://doi.org/10.1063/5.0254736

Optimal generation of mesoscopic twin-beam states by means of a natively femtosecond laser system

Cite as: APL Photon. 10, 036116 (2025); doi: 10.1063/5.0254736
Submitted: 24 December 2024 • Accepted: 4 March 2025 •
Published Online: 19 March 2025

View Online Export Citation CrossMark

A. Pozzoli,[1] M. Lamperti,[1,2] M. Clerici,[1] M. Bondani,[1,2] and A. Allevi[1,2,a)]

AFFILIATIONS

[1] Como Lake Institute of Photonics, Dipartimento di Scienza e Alta Tecnologia, Università degli Studi dell'Insubria, Via Valleggio 11, I-22100 Como, Italy
[2] Istituto di Fotonica e Nanotecnologie, IFN-CNR, Via Valleggio 11, I-22100 Como, Italy

[a)] **Author to whom correspondence should be addressed:** alessia.allevi@uninsubria.it

ABSTRACT

Mesoscopic twin-beam states, which exhibit robust nonclassical correlations, hold significant potential for applications in quantum technologies, including underwater quantum communication and quantum metrology. As Ytterbium-based lasers delivering sub-picosecond pulses are becoming the cornerstone of ultrafast photonics, optimizing the generation of quantum states of light driven by such short pulses while avoiding the presence of noise sources, such as spurious light, is also becoming essential. To this end, we propose an optical scheme that delivers well-populated entangled states in the red spectral region by pumping parametric down-conversion with optically tilted pulses, addressing the limited gain caused by group velocity mismatch between the driving pump field and the generated quantum radiation. The results obtained so far encourage the exploitation of this source in further optical schemes.

I. INTRODUCTION

The generation of mesoscopic entangled states could open interesting perspectives in the implementation of quantum technologies. For instance, it has been demonstrated that twin-beam (TWB) states, endowed with several photons, are robust against loss and noise,[1,2] thus being useful for different applications, including underwater quantum optical communication[3] and quantum metrology, such as imaging.[4–6] While the generation of such states with picosecond lasers is straightforward since the phase-matching (PM) condition in few-millimeter-long crystals can be easily achieved, the situation changes significantly with femtosecond laser systems, in which the group velocity mismatch (GVM) between the different spectral components of the laser pulse reduces the generation efficiency.[7,8] However, with sub-picosecond Yb-based lasers becoming the preferred solution for nonlinear photonics, it is essential to find an approach that efficiently delivers mesoscopic TWB states. To achieve this, it is crucial to design a source with parametric gain that is not limited by the natural splitting length of the pump and amplified radiation, which is typically on the order of hundreds of micrometers for 200 fs pump pulses in common nonlinear crystals.[8] Some years ago, it was shown that tilting the pump pulse is an effective strategy to address the GVM issue.[9] Since then, the use of pulse tilting has been widely employed in the context of nonlinear and quantum optics.[10] Pulse front tilt is routinely employed to achieve, for example, achromatic PM in nonlinear processes,[11–14] and for the efficient generation of THz pulses.[15] Pulse front tilt has also been employed in the context of quantum optics, for example, to control the joint spectrum of paired photons generated in spontaneous parametric down-conversion (PDC)[16–18] and to extend the bandwidth of biphoton fields.[19]

In this work, we demonstrate that pulse wavefront tilting allows for the generation of mesoscopic TWB states from <200 fs pump pulses in a condition where they could not be effectively generated otherwise due to the detrimental effect of GVM. In more detail, we show that, by linearly manipulating the femtosecond pulses at 347 nm of a Ytterbium laser, it is possible to eliminate the group velocity mismatch and avoid the presence of spurious light, thus

optimizing the production of mesoscopic TWB states. Their characterization is obtained both in the spectral and photon-number domains. For the latter, we used silicon photomultipliers (SiPMs), as they have been shown to be particularly suitable for the characterization of the quantum states[20] and possess a wide dynamic range.[21] We considered the noise reduction factor as the non-classicality criterion expressed in terms of measurable quantities. The results presented here are a stepping stone toward the ultimate goal of up-converting[22] the TWBs into the blue region,[23] where SiPMs exhibit even higher quantum efficiencies.

II. MATERIALS AND METHODS

A. Mitigation of GVM

PDC is a nonlinear quantum process that generates bipartite states of light, usually called TWBs, entangled in the number of photons.[24–26] It occurs when a field at frequency ω_3, called the pump, is injected into a $\chi^{(2)}$ crystal, where it interacts with the quantum vacuum fluctuations, thus producing two new sets of fields at frequencies ω_1 and ω_2, called the signal and idler. For efficient generation, both energy and PM conditions must be met.[27] While the former condition, that is, $\hbar\omega_3 = \hbar\omega_1 + \hbar\omega_2$, can lead to the production of a continuous frequency spectrum, the latter, that is, $\mathbf{k_3} = \mathbf{k_1} + \mathbf{k_2}$, causes each frequency to be generated in different directions. The realization of such a condition is typically achieved in birefringent crystals, such as β-barium borate (BBO), properly tuned either in angle or temperature, capable of guaranteeing a high level of transmittance over a wide range of frequencies. When driven by short pulsed localized beams, the PDC process is also affected by dispersion, diffraction, and the spatial walk-off occurring among the interacting waves within the nonlinear crystal. For instance, when the interacting pulses in a three-wave mixing process are shorter than a few picoseconds, the difference between the group velocities of the pump and generated fields plays a crucial role in defining the amplification bandwidth (both in frequency and angles, see, e.g., Ref. 28) and generally results in a reduction of the gain.[29] This effect can be easily understood by considering that amplification is effective only over a short propagation length (typically shorter than the crystal) known as the splitting length: $l_s = \tau\, c_0/|n_{g,p} - n_{g,s,z}|$, where $n_{g,p}$ is the pump group index, $n_{g,s,z}$ is the effective group index of the seed along the pump direction, and τ is the shortest pulse duration among the seed and the pump. This length measures the distance over which the pump and seed (or generally, the radiation at the signal frequency) separate due to GVM and the short pulse durations.

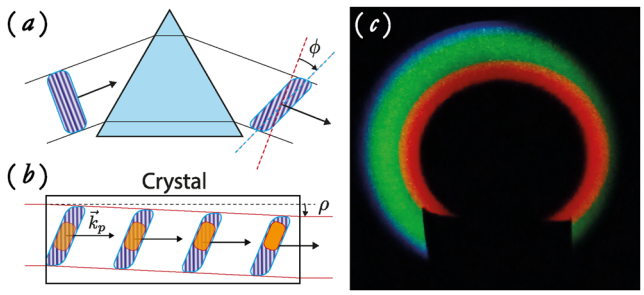

FIG. 1. (a) Sketch of the pulse front tilt ϕ acquired by the pump pulse crossing a dispersive prism. The shaded colors show the phase fronts. (b) Sketch of the combined effect of pulse front tilt and walk-off inside the nonlinear crystal, allowing matching of the pump and PDC group velocities. (c) Picture of a transverse section of the PDC cones in the visible spectral range produced by sending a pump beam roughly centered around 347 nm to a β-barium-borate crystal. The innermost red part corresponds to frequency degeneracy.

A solution to mitigate the impact of GVM on parametric amplification was proposed by Danielius *et al.*,[9] which relies on the combination of pump pulse front tilting and the spatial walk-off characteristic of birefringent crystals, see Figs. 1(a) and 1(b). This approach has been further investigated (see, e.g., Refs. 30 and 31) and has been broadly applied to optimize a wide range of parametric interactions (see, e.g., Refs. 32 and 33). The effects of pulse front tilting and the associated angular dispersion have also been considered as tools in quantum optics, see, e.g., Ref. 10, and references therein. As described in Ref. 9, the pump pulse front tilt combined with the crystal spatial walk-off results in a slower effective pump group velocity, matching those of the other interacting waves. This approach, in combination with non-collinear interaction geometry, has been shown to be very effective in counteracting the effect of GVM[30] and has been included as a tool in the SNLO software we employed to design our experiment.[34] In more detail, we investigated the parametric amplification of a non-collinear seed pulse at 694 nm by an intense UV pump at 347 nm, with a duration of ~190 fs, in a 4-mm-thick BBO crystal cut with the optical axis at $\simeq 33.8°$. The PM condition for the non-collinear interaction, with an external angle between the seed and the pump wave vectors of nearly 5° in the plane orthogonal to the principal plane of the crystal, is achieved by tuning the crystal angle. Since we consider a large pump beam, the gain is maximized within the splitting length $l_s \simeq 0.65$ mm, where we assume $n_{g,p} \simeq 1.783$ and $n_{g,s,z} = n_{g,s}/\cos\delta \simeq 1.696$, with $\delta \simeq 3°$ as the internal angle between the seed and pump wave vectors. It is clear that, with our experimental parameters, the gain will be much lower than what would be expected from the chosen nonlinear crystal when using longer pulses. Following the analysis in Ref. 30, it is possible to calculate the ideal tilt angle ϕ to impose on the pump for perfect group velocity matching among the interacting waves as

$$\phi = \arctan\left[\frac{1}{\tan\rho}\left(\frac{n_{g,p}}{n_{g,s,z}} - 1\right)\right] \simeq 35°, \tag{1}$$

where $\rho \simeq 4.21°$ is the walk-off angle at the chosen crystal tuning. Note that this internal tilt angle corresponds to an external tilt angle of $\phi_e = \arctan(n_{g,p}\tan\phi) \simeq 51.4°$. We imposed a tilt on the pump pulse by injecting the beam into a pair of UV-grade fused-silica equilateral prisms at the minimum deviation angle, then increased the resulting tilt to the desired value by demagnifying the beam with a telescope. Considering $n_{FS} \simeq 1.447$ and $n_{g,FS} \simeq 1.537$, the refractive and group indices for the 347 nm radiation in fused silica, respectively, the minimum deviation angle is $\beta_m \simeq 32.7°$. For a beam incident at the minimum deviation angle, the tilt produced by the equilateral prism at the output is given by[35,36]

$$\phi_e = \arctan\left(\lambda\frac{d\beta}{d\lambda}\right) \simeq \arctan\left(\lambda\frac{d\beta_m}{dn}\frac{dn}{d\lambda}\right) \simeq 7.43°, \tag{2}$$

where n is the material refractive index, and

$$\frac{d\beta_m}{dn} = -\frac{2\sin(\alpha/2)}{\cos[(\alpha-\beta_m)/2]}, \tag{3}$$

$$\frac{dn}{d\lambda} = \frac{n_{FS}-n_{g,FS}}{\lambda}, \tag{4}$$

in which $\alpha = 60^\circ$ is the prism angle. By cascading the two prisms, we achieved a tilt angle of $\phi_e \simeq 14.9^\circ$, and by demagnifying the beam with a telescope with magnification $M = 1/3$, we obtained $\phi_{e,m} = \arctan(\tan\phi_e/M) \simeq 38.5^\circ$. Although this tilt angle is not as large as the ideal one mentioned above, it is sufficient to increase the splitting length to a value larger than the crystal length:

$$l_{s,t} = \tau\frac{c_0}{|n_{g,p,t}-n_{g,s,z}|} \simeq 5.12\text{mm}, \tag{5}$$

where

$$n_{g,p,t} = \frac{n_{g,p}}{1+\tan\phi\,\tan\rho} \simeq 1.685. \tag{6}$$

B. Mesoscopic TWBs

Thanks to this strategy, we are able to produce bright and almost homogeneous TWB states, as can be easily appreciated in Fig. 1(c), which shows a picture of a transverse section of the PDC in the visible spectral range.

Since they are a multi-mode thermal field, they can be expressed in terms of the following density matrix:[37]

$$\rho^{\mu}_{\text{TWB}} = \sum_{n=0}^{\infty} P_{\text{mth}}(n)|n,n\rangle\langle n,n|, \tag{7}$$

in which

$$|n\rangle = \delta_{n,\left(\sum_{k=1}^{\mu} n_k\right)} \bigotimes_{k=1}^{\mu} |n_k\rangle_k, \tag{8}$$

and n is the overall number of photons, while $P_{\text{mth}}(n)$ is the multi-mode thermal photon-number distribution:[38]

$$P_{\text{mth}}(n) = \binom{n+\mu-1}{n}\left(\frac{\langle n\rangle}{\mu}\right)^n\left(1+\frac{\langle n\rangle}{\mu}\right)^{-n-\mu}, \tag{9}$$

where $\langle n\rangle$ is the mean number of photons in each arm and μ is the effective number of spatio-spectral modes under the assumption that they are equally populated.

Different criteria can be applied to test the non-classicality of such states.[39] In particular, some of them are particularly useful as they can be expressed in terms of measurable quantities.[40–44] We focus here on the calculation of the noise reduction factor, which is defined as the variance of the difference between the number of photons detected in the signal and idler arms normalized to the shot-noise level:[24,45]

$$R = \frac{\sigma^2(m_1-m_2)}{\langle m_1\rangle+\langle m_2\rangle}. \tag{10}$$

Values of R lower than 1 prove that the states are entangled in the number of photons.

This criterion is particularly useful for discriminating against the presence of spurious light collected together with TWBs and imperfections in the detection system. Indeed, the presence of such non-idealites can be included in the model, serving as an entangled source optimization tool. For instance, by assuming that a noise source is superimposed on one arm of the TWB and that there is an imbalance between signal and idler, the noise reduction factor reads as[2]

$$R = 1 - \frac{2\eta t\langle m\rangle}{(1+t)\langle m\rangle+\langle m_N\rangle} + \frac{(1-t)^2\langle m\rangle^2}{\mu[(1+t)\langle m\rangle+\langle m_N\rangle]} + \frac{\sigma^2(m_N)-\langle m_N\rangle}{(1+t)\langle m\rangle+\langle m_N\rangle}, \tag{11}$$

where $\langle m\rangle$ is the mean number of detected photons in a TWB arm, η is the global quantum efficiency of the detection system, $t \in (0,1)$ is the transmission efficiency quantifying the balancing between the two arms, while $\langle m_N\rangle$ and $\sigma^2(m_N)$ are the mean value and the variance of the noise source, respectively.

According to the specific nature of noise, the expression in Eq. (11) can assume different forms. For instance, in Ref. 2, it has been shown that coherent noise is less detrimental than a single-mode thermal one.

C. Experimental implementation

The source used to generate mesoscopic TWB states is the third harmonic of a Yb:KGW amplified laser emitting pulses centered at 347 nm with a repetition rate of 3 kHz and a transform-limited pulse duration of 190 fs. As shown in Fig. 2, the third-harmonic pulses are sent through a pair of prisms followed by a demagnifying imaging system. More specifically, a confocal telescope, composed of two lenses with focal lengths $f_1 = 300$ mm and $f_2 = 100$ mm, respectively, and placed 40 cm apart, is used to image the output face of the second prism onto the entrance face of the second-order nonlinear medium, namely, a BBO crystal of 4 mm thickness and cut at 33.8°.

Two twin portions of TWB around frequency degeneracy (~693 nm) are selected both spatially and spectrally by means of two irises (PH) and two band-pass filters (BF), respectively. These beams are then focused by achromatic doublets (AD) into multi-mode fibers (MF) with 1 mm core diameter and delivered to two SiPMs (mod. MPPC S13360–1350CS, Hamamatsu Photonics). These detectors, operating at room temperature, consist of a matrix of cells functioning in the Geiger–Müller regime with a common output. This model of SiPMs is characterized by a value of quantum efficiency, that is, ~16%@693 nm, but can reach higher values, that is, 40%, in the blue–green region.[46] After a preliminary fast amplification stage, the output signal is integrated over a 10 ns long gate to reduce the contributions of dark counts and optical cross-talk, which generally affect SiPMs.[47] Finally, the analog signals are digitized and acquired.

The pump energy is adjusted using two different means: attenuating the output energy of the fundamental beam from which the third harmonic is produced and employing a half-wave plate (HWP) followed by a polarizing cube beam splitter (PBS) applied to the

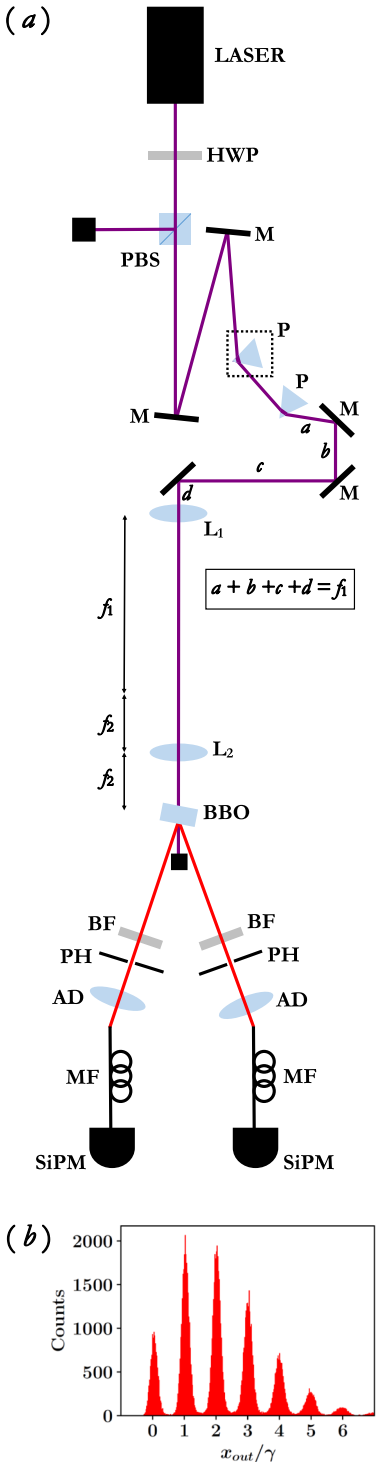

FIG. 2. (a): Sketch of the experimental setup: HWP, half-wave plate; PBS, polarizing cube beam splitter; M, mirror; P, prism; L_1 and L_2, lenses with focal lengths f_1 and f_2, respectively; BBO, β-barium-borate crystal; BF, band-pass filter; PH, pinhole; AD, achromatic doublet; MF, multi-mode fiber; SiPM, silicon photomultiplier. See the text for details. (b) Typical pulse height spectrum (PHS) obtained at the exit of the SiPM-based detection chain.

UV pump. This two-fold approach is aimed at revealing the possible presence of spurious light at increasing values of the pump power and at devising a valid method to avoid its emergence. Regarding the energy control of the HWP and PBS, it will later be shown that although the PBS is not strictly required due to the polarization sensitivity of the PDC process, it plays a crucial role in reducing spurious light, thereby optimizing the generation and detection of TWBs.

For each choice of the mean number of pump photons, 10^5 acquisitions are performed, corresponding to consecutive pump pulses. A typical pulse-height spectrum is shown in Fig. 2(b), from which it is clear that the employed detectors can resolve the number of photons.

III. RESULTS

Before analyzing the nonclassical nature of the produced TWB, we first focus on its spectral content. As mentioned in Sec. II C, the light detected in each arm is spectrally selected using a band-pass filter. In Fig. 3, we present the measured spectra. It can be observed that the spectra of the two arms are similar and roughly centered at 693 nm. This wavelength corresponds to twice that of the pump beam, whose spectrum is shown in the inset of the same figure. As will be demonstrated in the following sections, this configuration is the optimal one for the collection of non-classically correlated TWB states.

These collected portions are characterized by a multi-mode thermal distribution of the number of photons. To prove this, we process the data acquired by the SiPMs in each arm for every mean value of the pump and divide the results by the mean distance between consecutive peaks of the pulse height spectrum (PHS), which roughly corresponds to the gain of the detection system indicated as γ in Fig. 2(b). We then rebin the resulting numbers into unitary bins.[21] The statistical distributions of these rebinned numbers represent the distributions of detected photons. As an

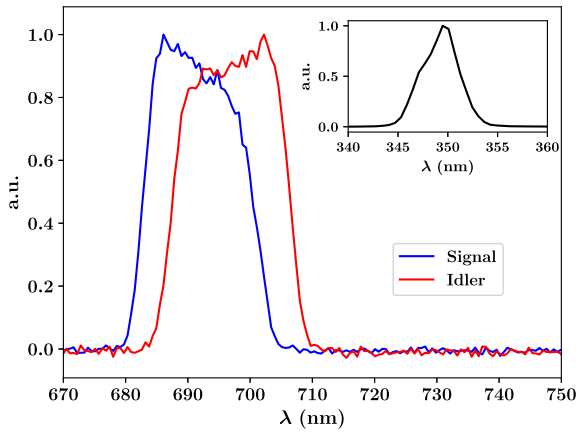

FIG. 3. Main: spectra normalized to the maximum corresponding to the light collected in the two arms of TWB. The blue curve corresponds to the signal arm, while the red curve corresponds to the idler arm. Inset: spectrum of the pump beam at the exit of the system of two prisms.

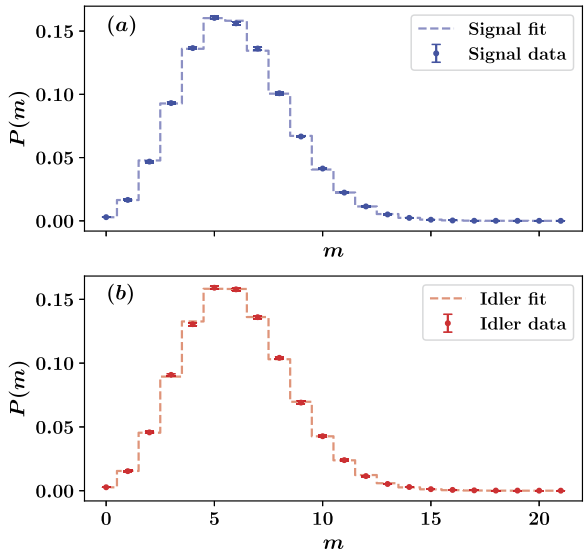

FIG. 4. Typical photon-number distributions measured in the signal arm [blue dots, panel (a)] and the idler arm [red dots, panel (b)] superimposed on the multi-mode thermal fitting functions of Eq. (9). The mean value of the number of photons is $\langle m \rangle = 5.95$ in both arms. The free fitting parameter is the number of modes, which is equal to $\mu = 193 \pm 29$ in the signal arm and $\mu = 190 \pm 26$ in the idler arm.

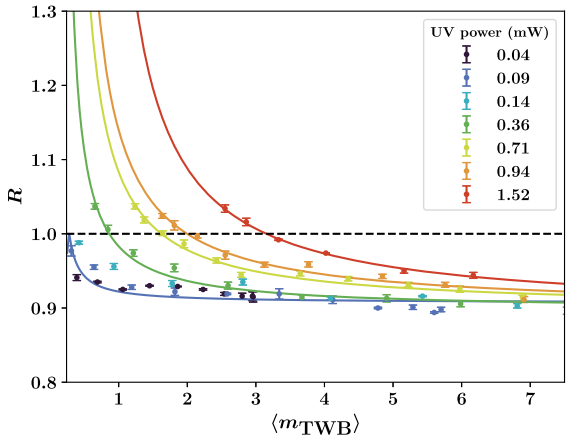

FIG. 5. R as a function of the mean value of the signal arm for different energy values of the fundamental beam of the laser system in the absence of the PBS in the pump beam path. Colored dots represent experimental data, while colored curves represent theoretical expectations according to Eq. (11) under the assumption of either coherent or thermal noise. The fitting parameters are $\eta = 0.093 \pm 0.005$ and $\langle m_N \rangle = 0.28 \pm 0.03$ for $P_{UV} = 0.04$, 0.09, and 0.14 mW, $\eta = 0.102$, $\langle m_N \rangle = 0.33$, and $\mu_N = 1.00$ for $P_{UV} = 0.36$ mW, $\eta = 0.102$, $\langle m_N \rangle = 0.48$, and $\mu_N = 1.00$ for $P_{UV} = 0.71$ mW, $\eta = 0.102$, $\langle m_N \rangle = 0.55$, and $\mu_N = 1.01$ for $P_{UV} = 0.94$ mW, $\eta = 0.107$, $\langle m_N \rangle = 1.20$, and $\mu_N = 3.42$ for $P_{UV} = 1.52$ mW. The black dashed line corresponds to the threshold condition $R = 1$.

example, in Fig. 4, we show with colored dots the reconstructed photon number distribution for the signal (a) and idler (b), together with the corresponding theoretical predictions from Eq. (9) (dashed curves).

Given this preliminary characterization, the optimization of the entangled source is studied in terms of the noise reduction factor. As mentioned in the introduction, two crucial aspects have been considered. On one hand, the two-prism configuration is necessary to reduce the GV mismatch, as anticipated in the theoretical section. This aspect will be addressed in greater detail in Sec. III B. On the other hand, the use of the PBS is crucial to minimize spurious noise.

A. Contrasting spurious light

To highlight this second point, in Fig. 5, we show the noise reduction factor, R, as a function of the mean value measured in the signal arm without the PBS, for different mean values of the pump beam. It can be seen that the higher the mean value of the pump power, the more challenging it becomes to measure nonclassical correlations. Indeed, as the pump power increases, the R values exceed 1, particularly at lower values of the TWB mean photon numbers. Since the energy variation was obtained by rotating the half-wave plate, at decreasing mean values of the photon number the amount of spurious light (e.g., fluorescence of pump light scattered inside the crystal) becomes more significant. To better emphasize the presence of spurious light superimposed on the experimental data, we show the theoretical expectations according to Eq. (11) under the assumption of thermal noise as colored curves. The fit parameters provided in the caption of the figure prove the presence of thermal noise, which increases with increasing the pump mean values. Since its contribution is definitely detrimental to the optimization of the setup, we chose to investigate what happens by adding a PBS beyond the half-wave plate. In Fig. 6, we show the corresponding noise reduction factor as a function of the mean value measured in the signal arm for different mean values of the pump beam. Data corresponding to different attenuations of the fundamental beam, and thus to different UV pump values, are almost superimposed on the same theoretical expectation, confirming the absence of spurious

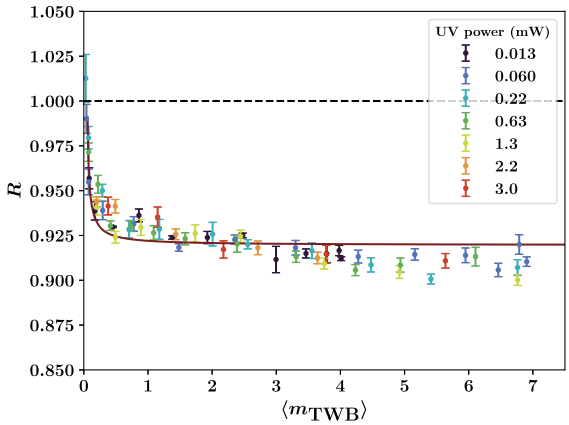

FIG. 6. R as a function of the mean value of the signal arm for different energy values of the fundamental beam of the laser system and in the presence of the PBS in the pump beam path. Colored dots: experimental data; black curve: theoretical expectation according to Eq. (11). The fitting parameters are $\eta = 0.080 \pm 0.002$ and $\langle m_N \rangle = 0.059 \pm 0.008$. The black dashed line corresponds to the threshold condition $R = 1$.

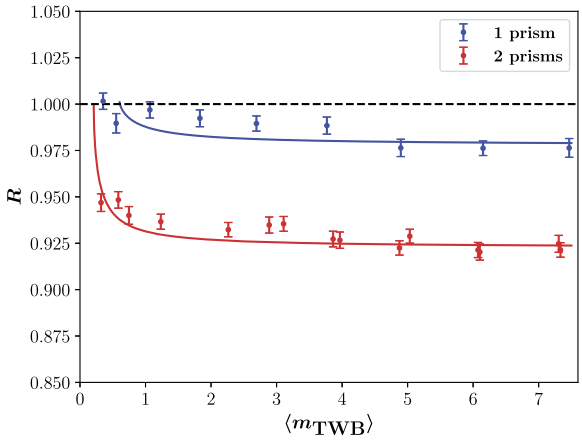

FIG. 7. R as a function of the mean value of the signal arm in the presence of the PBS in the pump beam path. Blue (red) dots correspond to experimental data obtained with the 1-prism(2-prisms) configuration, while colored curves correspond to the theoretical expectations according to Eq. (11). The fitting parameters are $\eta = 0.077 \pm 0.002$ and $\langle m_N \rangle = 0.21 \pm 0.04$ for the red curve, and $\eta = 0.022 \pm 0.002$ and $\langle m_N \rangle = 0.60 \pm 0.04$ for the blue curve. The black dashed line corresponds to the threshold condition $R = 1$.

light. Moreover, we highlight that the constant value of R reached for small mean values (<0.5) indicates that the signal and idler are well balanced and gives information about the effective quantum efficiency of the detection chain, which is equal to $\eta = 0.08$. This value is smaller than the quantum efficiency of the employed SiPMs in the red spectral region (~0.15), as it also includes possible inefficiencies due, for example, to fiber coupling. Finally, we note that the larger values of R at low mean photon numbers are due to the increasing impact of dark counts at low detection rates.

B. Reduction of GVM

All the measurements presented so far have been obtained using the two-prism configuration on the pump-beam path. This strategy enables the compensation of GVM, as already explained in Sec. II. To demonstrate the importance of introducing such a system, we measured the noise reduction factor achieved using only one prism and compared it with that obtained with the two-prism configuration. For the first case, a high-reflectivity mirror was used instead of the prism to keep the setup aligned. In Fig. 7, we compare the results obtained in the two configurations. It is evident that the compensation of the GVM plays a key role in the level of non-classicality that can be achieved. In fact, the values of R obtained in the one-prism configuration are much closer to 1, revealing a less efficient generation of quantum states of light, as also proved by the value of η that can be obtained from the fitting procedure.

IV. DISCUSSION

The results shown in the previous sections highlight that, by properly operating on the pump beam, it is possible to efficiently generate TWB states by mitigating the impact of GVM and reducing the presence of spurious light. The proposed optimization strategies are crucial for operating in the red spectral range, specifically at frequency degeneracy, that is, at ~693 nm. The uniformity of the obtained TWB states has been quantitatively checked by analyzing the spectrum around the collected wavelength. The efficiency of the produced TWB has also been investigated in terms of photon numbers. In particular, through the reconstruction of the detected-photon distributions and the calculation of non-classicality criteria, we have proved that the obtained TWB states are multi-mode thermal and sub-shot-noise correlated, respectively. We note that the presence of tens of modes makes the detection of nonclassical correlations easier. In fact, as it can be appreciated by looking at Eq. (11), the larger the number of modes μ, the less detrimental the possible presence of some imbalance between the two arms. Moreover, we emphasize that in optimizing the setup, we focused our attention on avoiding the presence of spurious light while minimizing the number of elements used to prepare the pump beam. In particular, we have shown that the noise reduction factor itself represents a powerful tool, as it allows us to determine the amount of noise and also its nature. Furthermore, it is a valuable strategy to test the adopted 2-prism configuration to reduce GVM. All these considerations lead us to continue the investigation of the possible exploitation of the generated source in further optical schemes.

V. CONCLUSIONS

In this work, we presented the step-by-step optimization and characterization of mesoscopic TWB states produced by a femtosecond laser system. More specifically, we mitigated the GVM effect, obtaining sharp and bright PDC cones. Moreover, we investigated the possible presence of spurious light and identified the best strategy to eliminate it while collecting the proper twin portions of light. The non-classicality of the optimized TWB was verified by adopting a non-classicality criterion based solely on measurable quantities. The next step will involve the up-conversion of these two portions in the blue spectral region to generate non-classically correlated states to be used for underwater quantum communication.

ACKNOWLEDGMENTS

M.L. and A.A. acknowledge support from Grant No. PNRR D.D.M.M. 737/2021. M.C. and M.B. acknowledge support from Project No. PRIN 2022K3KMX7 of the MUR, Grant No. CUP B53D23005150006. This work was also funded by PNRR MUR Project No. PE0000023-NQSTI.

AUTHOR DECLARATIONS

Conflict of Interest

The authors have no conflicts to disclose.

Author Contributions

A. Pozzoli: Data curation (equal); Formal analysis (equal); Writing – review & editing (equal). **M. Lamperti**: Data curation (equal);

Methodology (equal); Writing – review & editing (equal). **M. Clerici**: Conceptualization (equal); Methodology (equal); Software (equal); Writing – original draft (equal); Writing – review & editing (equal). **M. Bondani**: Conceptualization (equal); Methodology (equal); Writing – review & editing (equal). **A. Allevi**: Conceptualization (equal); Data curation (equal); Methodology (equal); Writing – original draft (equal); Writing – review & editing (equal).

DATA AVAILABILITY

The data that support the findings of this study are available from the corresponding author upon reasonable request.

REFERENCES

[1] A. Allevi and M. Bondani, "Preserving nonclassical correlations in strongly unbalanced conditions," J. Opt. Soc. Am. B **36**(12), 3275–3281 (2019).
[2] A. Allevi and M. Bondani, "Effect of noisy channels on the transmission of mesoscopic twin-beam states," Opt. Express **29**(21), 32842–32852 (2021).
[3] A. Allevi and M. Bondani, "Towards underwater quantum communication in the mesoscopic intensity regime," Opt. Express **30**(24), 44175–44185 (2022).
[4] O. Wolley, T. Gregory, S. Beer, T. Higuchi, and M. Padgett, "Quantum imaging with a photon counting camera," Sci. Rep. **12**, 8286 (2022).
[5] G. Ortolano, A. Paniate, P. Boucher, C. Napoli, S. Soman, S. F. Pereira, I. Ruo-Berchera, and M. Genovese, "Quantum enhanced non-interferometric quantitative phase imaging," Light: Sci. Appl. **12**, 171 (2023).
[6] F. Picariello, E. Losero, D. Tchernij, P. Boucher, M. Genovese, I. Ruo-Berchera, and I. P. Degiovanni, "Quantum super-resolution microscopy by photon statistics and structured light," arXiv:2408.11654v1.
[7] I. Tomov, R. Fedosejevs, and A. Offenberger, "Up-conversion of subpicosecond light pulses," IEEE J. Quantum Electron. **18**(12), 2048–2056 (1982).
[8] A. V. Gorbach, M. Roiz, M. Vainio, and D. V. Skryabin, "Trapping of ultrashort pulses in nondegenerate parametric conversion," Phys. Rev. A **107**, 063515 (2023).
[9] R. Danielius, P. Di Trapani, C. Solcia, P. Foggi, A. Andreoni, and A. Piskarskas, "Matching of group velocities by spatial walk-off in collinear three-wave interaction with tilted pulses," Opt. Lett. **21**(13), 973–975 (1996).
[10] J. P. Torres, M. Hendrych, and A. Valencia, "Angular dispersion: An enabling tool in nonlinear and quantum optics," Adv. Opt. Photonics **2**, 319–369 (2010).
[11] V. D. Volosov, S. G. Karpenko, N. E. Kornienko, and V. L. Strizhevskii, "Method for compensating the phase-matching dispersion in nonlinear optics," Sov. J. Quantum Electron. **4**, 1090 (1975).
[12] O. E. Martinez, "Achromatic phase matching for second harmonic generation of femtosecond pulses," IEEE J. Quantum Electron. **25**, 2464–2468 (1989).
[13] A. Dubietis, G. Valiulis, G. Tamošauskas, R. Danielius, and A. Piskarskas, "Nonlinear second-harmonic pulse compression with tilted pulses," Opt. Lett. **22**, 1071–1073 (1997).
[14] B. A. Richman, S. E. Bisson, R. Trebino, E. Sidick, and A. Jacobson, "Efficient broadband second-harmonic generation by dispersive achromatic nonlinear conversion using only prisms," Opt. Lett. **23**, 497–499 (1998).
[15] J. Hebling, G. Almási, I. Z. Kozma, and J. Kuhl, "Velocity matching by pulse front tilting for large-area THz-pulse generation," Opt. Express **10**, 1161–1166 (2002).
[16] J. P. Torres, F. Macià, S. Carrasco, and L. Torner, "Engineering the frequency correlations of entangled two-photon states by achromatic phase matching," Opt. Lett. **30**, 314–316 (2005).
[17] M. Hendrych, M. Micuda, and J. P. Torres, "Tunable control of the frequency correlations of entangled photons," Opt. Lett. **32**, 2339–2341 (2007).
[18] X. Shi, A. Valencia, M. Hendrych, and J. P. Torres, "Generation of indistinguishable and pure heralded single photons with tunable bandwidth," Opt. Lett. **33**, 875–877 (2008).
[19] M. Hendrych, X. Shi, A. Valencia, and J. P. Torres, "Broadening the bandwidth of entangled photons: A step towards the generation of extremely short biphotons," Phys. Rev. A **79**, 023817 (2009).
[20] G. Chesi, L. Malinverno, A. Allevi, R. Santoro, M. Caccia, and M. Bondani, "Measuring nonclassicality with silicon photomultipliers," Opt. Lett. **44**(6), 1371–1374 (2019).
[21] S. Cassina, A. Allevi, V. Mascagna, M. Prest, E. Vallazza, and M. Bondani, "Exploiting the wide dynamic range of silicon photomultipliers for quantum optics applications," EPJ Quantum Technol. **8**, 4 (2021).
[22] I. I. Arkhipov, J. Peřina, Jr., O. Haderka, A. Allevi, and M. Bondani, "Entanglement and nonclassicality in four-mode Gaussian states generated via parametric down- conversion and frequency up-conversion," Sci. Rep. **6**, 33802 (2016).
[23] A. Allevi and M. Bondani, "Feasibility of a novel quantum communication protocol in Jerlov type I water," Entropy **25**, 16 (2022).
[24] A. Heidmann, R. J. Horowicz, S. Reynaud, E. Giacobino, C. Fabre, and G. Camy, "Observation of quantum noise reduction on twin laser beams," Phys. Rev. Lett. **59**(22), 2555–2557 (1987).
[25] R. Loudon, *The Quantum Theory of Light*, 3rd ed. (Oxford Science, 2000).
[26] U. Leonhardt, *Essential Quantum Optics* (Cambridge University Press, Cambridge, 2010).
[27] R. W. Boyd, *Nonlinear Optics*, 3rd ed. (Elsevier, Amsterdam, 2008).
[28] M. Clerici, O. Jedrkiewicz, E. Rubino, D. Faccio, L. Tartara, V. Degiorgio, and P. D. Trapani, "Generation and amplification of pulsed Bessel beams by seeding an optical parametric amplifier," Opt. Lett. **33**(20), 2296–2298 (2008).
[29] A. Kobyakov, E. Schmidt, and F. Lederer, "Effect of group-velocity mismatch on amplitude and phase modulation of picosecond pulses in quadratically nonlinear media," J. Opt. Soc. Am. B **14**(11), 3242–3252 (1997).
[30] A. V. Smith, "Group-velocity-matched three-wave mixing in birefringent crystals," Opt. Lett. **26**(10), 719–721 (2001).
[31] D. N. Schimpf, J. Rothhardt, J. Limpert, A. Tünnermann, and D. C. Hanna, "Theoretical analysis of the gain bandwidth for noncollinear parametric amplification of ultrafast pulses," J. Opt. Soc. Am. B **24**(11), 2837–2846 (2007).
[32] F. Wagner, M. Feuerhake, and P. Simon, "Group-velocity-dispersion- compensated femtosecond optical parametric amplifier," Opt. Quantum Electron. **29**, 811–818 (1997).
[33] K. S. Wong, Z. R. Qui, H. Wang, and G. K. L. Wong, "Efficient visible femtosecond optical parametric generator and amplifier using tilted pulse-front pumping," Opt. Lett. **22**(12), 898–900 (1997).
[34] A. V. Smith, Snlo Version 75.2.2 Nonlinear Optics Code, AS-Photonics, Albuquerque, NM (2021).
[35] Z. Bor and B. Rácz, "Group velocity dispersion in prisms and its application to pulse compression and travelling-wave excitation," Opt. Commun. **54**(3), 165–170 (1985).
[36] J.-C. Diels and W. Rudolph, *Ultrashort Laser Pulse Phenomena* (Academic Press, 2006).
[37] A. Allevi and M. Bondani, "Multi-mode twin-beam states in the mesoscopic intensity domain," Phys. Lett. A **423**, 127828 (2022).
[38] L. Mandel and E. Wolf, *Optical Coherence and Quantum Optics* (Cambridge University Press, Cambridge, UK, 1995).
[39] J. Peřina, P. Pavlíček, V. Michálek, R. Machulka, and O. Haderka, "Nonclassicality criteria for *N*-dimensional optical fields detected by quadratic detectors," Phys. Rev. A **105**, 013706 (2022).
[40] W. Vogel, "Nonclassical correlation properties of radiation fields," Phys. Rev. Lett. **100**, 013605 (2008).
[41] J. Peřina, I. I. Arkhipov, V. Michálek, and O. Haderka, "Nonclassicality and entanglement criteria for bipartite optical fields characterized by quadratic detectors," Phys. Rev. A **96**, 043845 (2017).

[42]J. Peřina, V. Michalek, and O. Haderka, "Nonclassicality and entanglement criteria for bipartite optical fields characterized by quadratic detectors. II. Criteria based on probabilities," Phys. Rev. A **102**, 043713 (2020).
[43]G. Brida, M. Bondani, I. P. Degiovanni, M. Genovese, M. G. A. Paris, I. Ruo Berchera, and V. Schettini, "On the discrimination between classical and quantum states," Found. Phys. **41**, 305–316 (2011).
[44]A. Allevi, S. Olivares, and M. Bondani, "Measuring high-order photon-number correlations in experiments with multimode pulsed quantum states," Phys. Rev. A **85**, 063835 (2012).
[45]A. Agliati, M. Bondani, A. Andreoni, G. D. Cillis, and M. G. A. Paris, "Quantum and classical correlations of intense beams of light investigated via joint photodetection," J. Opt. B: Quantum Semiclassical Opt. **7**(12), S652–S663 (2005).
[46]See https://www.hamamatsu.com/content/dam/hamamatsu-photonics/sites/documents/99_SALES_LIBRARY/ssd/s13360_series_kapd1052e.pdf for information about MPPC S13360-1350CS.
[47]G. Chesi, L. Malinverno, A. Allevi, R. Santoro, M. Caccia, A. Martemiyanov, and M. Bondani, "Optimizing silicon photomultipliers for quantum optics," Sci. Rep. **9**, 7433 (2019).